

DeDPO: Debiased Direct Preference Optimization for Diffusion Models

Khiem Pham^{1*} Quang Nguyen^{2*} Tung Nguyen^{1*} Jingsen Zhu¹ Michele Santacatterina³
 Dimitris Metaxas² Ramin Zabih¹
¹Cornell University ²Rutgers University ³NYU

Abstract

Direct Preference Optimization (DPO) has emerged as a predominant alignment method for diffusion models, facilitating off-policy training without explicit reward modeling. However, its reliance on large-scale, high-quality human preference labels presents a severe cost and scalability bottleneck. To overcome this, We propose a semi-supervised framework augmenting limited human data with a large corpus of unlabeled pairs annotated via cost-effective synthetic AI feedback. Our paper introduces Debiased DPO (DeDPO), which uniquely integrates a debiased estimation technique from causal inference into the DPO objective. By explicitly identifying and correcting the systematic bias and noise inherent in synthetic annotators, DeDPO ensures robust learning from imperfect feedback sources, including self-training and Vision-Language Models (VLMs). Experiments demonstrate that DeDPO is robust to the variations in synthetic labeling methods, achieving performance that matches and occasionally exceeds the theoretical upper bound of models trained on fully human-labeled data. This establishes DeDPO as a scalable solution for human-AI alignment using inexpensive synthetic supervision.

1. Introduction

Text-to-image diffusion models have demonstrated impressive capabilities in generating photorealistic and semantically consistent images from natural language prompts [9, 15, 44]. These models are typically trained with supervised learning on large-scale image-text datasets [47], which enables broad generalization but offers limited control over fine-grained image attributes valued by users, such as prompt adherence or aesthetic quality. As a result, generated outputs may often diverge from user intent despite textual relevance.

To bridge this gap, preference-based alignment methods have been developed to fine-tune generative models with human feedback. In language models, Reinforce-

ment Learning from Human Feedback (RLHF) [18, 37] has proven effective by training a reward model on pairwise human annotations and applying policy-gradient methods [36, 48] for fine-tuning. Similar RL-based strategies have been extended to image generation [3, 11], where diffusion models are optimized using rewards derived from human judgments. However, these methods incur substantial computational costs due to the need to train and maintain a separate reward model. To mitigate this, Direct Preference Optimization (DPO) [42] was introduced to directly fine-tune language models on human preference pairs, eliminating the reward model requirement. Building on this success, Diffusion-DPO [57] extends DPO to text-to-image diffusion models, achieving efficient human alignment. This approach has since been adapted to various generative tasks, including image inpainting [50], video generation [31, 61], and physically grounded 3D generation [29].

Despite its effectiveness, DPO-based methods face a key challenge: acquiring large-scale human preference labels is prohibitively expensive and time-consuming, limiting scalability. To address this, recent efforts have explored using synthetic preferences as a cheaper alternative [14, 25]. However, such feedback may diverge from human judgment, introduce noise, and cause instability during training. Other approaches attempt to create synthetic preferences by degrading high-quality images [39], but the lack of real human supervision can cause misalignment and limit effectiveness. In essence, directly training on AI-generated or synthetic preferences can be seen as learning from misaligned or noisy feedback, which undermines the reliability of alignment.

To address this problem, we propose **DeDPO**, a simple yet effective method that combines DPO with a debiased estimator to improve the training stability and robustness to imperfect feedback. DeDPO retains the desirable properties of DPO, training with completely offline data, while simultaneously achieving robustness to potential errors in synthetic preferences. Our method achieves performance equal to, and sometimes incrementally better than DPO trained on fully labeled data, even when only a small set of high-quality human preferences is available alongside a larger

*Equal contribution.

set of potentially noisy synthetic preferences. Experiments demonstrate that DeDPO consistently improves alignment quality and robustness in settings where human feedback is scarce and synthetic feedback is unreliable, offering a scalable path to aligning diffusion models with human values.

2. Related Work

Alignment by synthetic preferences. Synthetic preferences for DPO can be obtained from two types of models: reward models trained on large datasets of preference pairs (e.g., PickScore [24], HPSv2 [60]), and pretrained vision-language models (e.g., CLIP [41], Aesthetic [46]) that were not specifically trained on preference data. The original Diffusion-DPO [57] proposes using both types of these synthetic preferences. Recent work [20] uses reward models to label synthetically generated image pairs for DPO training as a scalable approach for learning from online data. However, this approach inherently assumes access to a large dataset of labeled preference pairs, *whereas we consider a more realistic setting with only a small set of labeled pairs and a larger set of unlabeled pairs*. Therefore, the most relevant approach to our work is the second one, which utilizes pretrained vision-language models that were not trained on preference pairs. Another line of work by Yuan et al. [68] uses self-play: the diffusion model iteratively competes against its own earlier versions to improve alignment. These approaches (self-play or pretrained-model feedback) motivate our focus on data-efficient alignment without large human datasets. Beyond text-to-image generation, there is a plethora of works using multimodal synthetic data to train large vision-language models [8, 26–28, 30, 58, 69]. These typically distill knowledge from responses of much larger models such as ChatGPT and Gemini. However, to our knowledge, there is no prior work on using multimodal models to generate preference labels for DPO training.

Robust alignment with noisy labels. AI feedback (synthetic preference) may be noisy and inconsistent with real human preference, leading to unstable alignment, so it is crucial to develop a robust alignment strategy against noisy preference labels. Existing work largely follows two directions. The first line assumes a parametric noise model on the labels [4, 7, 35]. For instance, Mitchell [35] introduce a conservative variant of DPO by smoothing the binary labels (analogous to label smoothing [54]), and Chowdhury et al. [7] further debias this loss and analyze its sub-optimality gap. A second line uses distributionally robust optimization (DRO) [22, 34, 59, 63], either by reweighting DPO gradients to approximate a robust objective [63] or by adding gradient regularization terms [34]. In contrast, we do not assume a specific noise model and, crucially, we assume access to only a small set of high-quality human prefer-

ence labels. This reference set allows us to correct bias in AI feedback rather than optimizing for worst-case noise alone. Moreover, prior robust DPO work focuses on language models, while we study robustness for visual generation. Related approaches in RLHF learn robust reward models [5, 13, 38, 64, 66], whereas our method remains reward-model-free and directly tackles noisy labels from pretrained models.

Doubly Robust / Debiased estimators. Doubly Robust / Debiased estimators originated in the missing-data and causal-inference literature [2, 43, 45] and have since been applied to off-policy reinforcement learning [10, 19, 56] and causal machine learning [6]. The key idea is to combine two nuisance models that target the same quantity into a meta-estimator that remains consistent if *either* model is correctly specified, and attains semi-parametric efficiency when they are both sufficiently accurate [6, 12, 21]. When used as a loss, such debiased objectives yield efficient parameter estimation. Closest to our setting, these ideas have been used for semi-supervised classification [70] by treating pseudo-labels as noisy surrogates of missing labels and designing a debiased loss robust to pseudo-label errors. However, they neither leverage AI feedback from external models nor enforce sample splitting, which is crucial for unbiased and efficient debiased estimation (see our method section). More recently, Xu et al. [62] apply these techniques to robustly align large language models, but their algorithm requires online data generation, departing from the fully offline nature of DPO. In contrast, we integrate debiased estimation directly into preference optimization for diffusion models, improving robustness to synthetic, noisy preferences while preserving the offline training setting.

3. Preliminaries

Text-to-image diffusion model. Diffusion models [9, 17, 44, 52, 53] generate images by learning to reverse a gradual noising process applied to image latents. Formally, they model the transformation from a standard Gaussian noise map $\epsilon \sim \mathcal{N}(0, \mathbf{I})$ to a sample from the target data distribution via a denoising diffusion process. The forward (noising) process perturbs a clean image latent \mathbf{x}_0 across multiple timesteps t as:

$$\mathbf{x}_t = \alpha_t \mathbf{x}_0 + \sigma_t \epsilon, \quad (1)$$

where α_t and σ_t are time-dependent scaling coefficients satisfying $\alpha_0 = \sigma_T = 1$ and $\alpha_T = \sigma_0 = 0$. The reverse process learns to recover \mathbf{x}_0 by denoising \mathbf{x}_t using a noise estimator ϵ_θ , trained to predict the noise ϵ via:

$$\min_{\theta} \mathbb{E}_{t \sim \mathcal{U}(0, T), \epsilon \sim \mathcal{N}(0, \mathbf{I})} \|\epsilon_\theta(\mathbf{x}_t, t) - \epsilon\|_2^2. \quad (2)$$

In the text-to-image setting, models are further conditioned on text embeddings \mathbf{c} , modifying the noise predictor to $\epsilon_\theta(\mathbf{x}_t, t, \mathbf{c})$. This conditioning enables the generation to be guided by textual prompts. To strengthen alignment between the image and the text, many models incorporate classifier-free guidance (CFG) [9, 16], which blends conditional and unconditional predictions using a guidance scale γ . The guided output is computed as:

$$\hat{\epsilon}_\theta(\mathbf{x}_t, t, \mathbf{c}) = \epsilon_\theta(\mathbf{x}_t, t) + \gamma (\epsilon_\theta(\mathbf{x}_t, t, \mathbf{c}) - \epsilon_\theta(\mathbf{x}_t, t)), \quad (3)$$

where $\epsilon_\theta(\mathbf{x}_t, t, \mathbf{c})$ denotes the prediction conditioned on the text, and $\epsilon_\theta(\mathbf{x}_t, t)$ denotes the unconditional prediction. CFG enhances both the fidelity and semantic relevance of generated images without relying on an external classifier.

DPO for text-to-image diffusion models. Direct Preference Optimization (DPO) [42] offers an efficient alternative to reward modeling for aligning generative models with human preferences. Diffusion-DPO [57] extends this approach to text-to-image diffusion models by adapting the DPO objective to the denoising process. Since diffusion models generate images through a sequence of latent states over T timesteps, directly computing the full trajectory likelihood is intractable. To address this, Diffusion-DPO proposes a surrogate loss based on denoising score comparisons at individual timesteps. For a given text prompt \mathbf{c} and an image pair $(\mathbf{x}_t^w, \mathbf{x}_t^l)$ annotated by human preference $\mathbf{x}_t^w \succ \mathbf{x}_t^l$, with Gaussian noise samples $(\epsilon^w, \epsilon^l) \sim \mathcal{N}(0, \mathbf{I})$, the preference loss is approximated as:

$$\mathcal{L}_{\text{DPO}}(\theta) = \mathbb{E}_{t, \mathbf{c}, \mathbf{x}_t^w, \mathbf{x}_t^l} [-\log \mathcal{G}_\theta(\mathbf{c}, \mathbf{x}_t^l, \mathbf{x}_t^w)], \quad (4)$$

$$\text{where } \mathcal{G}_\theta(\mathbf{c}, \mathbf{x}_t^l, \mathbf{x}_t^w) =$$

$$\sigma \left(-\beta (\|\epsilon^w - \epsilon_\theta(\mathbf{x}_t^w, t)\|_2^2 - \|\epsilon^w - \epsilon_{\text{ref}}(\mathbf{x}_t^w, t)\|_2^2 \right. \\ \left. - \|\epsilon^l - \epsilon_\theta(\mathbf{x}_t^l, t)\|_2^2 + \|\epsilon^l - \epsilon_{\text{ref}}(\mathbf{x}_t^l, t)\|_2^2 \right)$$

where $\sigma(\cdot)$ is the sigmoid function, \mathbf{x}_t^w and \mathbf{x}_t^l are the noise-perturbed images at timestep t (Eq. (1)), ϵ_θ is the trainable noise predictor and ϵ_{ref} is a frozen reference model. This formulation encourages the model to improve denoising quality on preferred samples relative to less preferred ones, effectively aligning generation with preference signals without relying on reward modeling. It also regularizes the model to stay close to the reference model [42].

4. Method

Problem setting. Due to the high cost of acquiring human preference labels, we consider a semi-supervised DPO setting with a small labeled set of text-to-image pairs and a larger unlabeled set. For the latter, we use AI feedback to generate synthetic preference labels.

DPO as binary classification. We first re-interpret DPO in Eq. (4) as an equivalent binary classification problem. For an *unordered* image pair $(\mathbf{x}^0, \mathbf{x}^1)$ with text prompt \mathbf{c} , we denote \mathbf{z} as the preference label over the pair, where $\mathbf{z} = 1$ denotes preference on \mathbf{x}^1 and $\mathbf{z} = 0$ otherwise. With this label, we can rewrite the loss in Eq. (4) as a binary cross-entropy loss

$$\mathcal{L}_{\text{DPO}}(\theta) = \mathbb{E}_{t, \mathbf{c}, \mathbf{x}_t^0, \mathbf{x}_t^1} [\mathcal{L}(\mathcal{G}_\theta(\mathbf{c}, \mathbf{x}_t^0, \mathbf{x}_t^1), \mathbf{z})], \quad (5)$$

where $\mathcal{L}(a, b) = -b \log a + (1 - b) \log(1 - a)$

which is a binary classification loss with predictive model $\hat{\mathbf{z}} = \mathcal{G}_\theta(\mathbf{c}, \mathbf{x}_t^0, \mathbf{x}_t^1)$ and target label \mathbf{z} .

Notes on symbols. We drop the subscript t for brevity. For example, \mathbf{x}_t^0 is written as \mathbf{x}^0 . We also drop the subscripts of the expectation operator \mathbb{E} . \mathbb{E}_n denotes the average over n samples (equivalent to the operator $\frac{1}{n} \sum_{i=1}^n \cdot$). \mathbf{y} denotes the input triplet $\mathbf{y} = (\mathbf{c}, \mathbf{x}^0, \mathbf{x}^1)$. Therefore, Eq. (5) can be written as:

$$\mathcal{L}_{\text{DPO}}(\theta) = \mathbb{E}_n \mathcal{L}(\mathcal{G}_\theta(\mathbf{y}), \mathbf{z}) \quad (6)$$

We will slightly overload \mathcal{G} to mean any mapping from the input \mathbf{y} to the label prediction $\hat{\mathbf{z}}$, reserving \mathcal{G}_θ for the model’s implicit margin (Eq. (4)). Additionally, we note that the expectation is also taken over the denoising time t .

Towards a semi-supervised approach. With our semi-supervised setting, let \mathbf{y}_l and \mathbf{y}_u be the labeled and unlabeled data, and n_l and n_u be the number of labeled and unlabeled samples. For the unlabeled data, we generate *synthetic preference* labels $\hat{\mathcal{G}}(\mathbf{y}_u)$ by some cheap but possibly incorrect annotator $\hat{\mathcal{G}}$. A straightforward and naive solution to solve the semi-supervised problem is to use the empirical average loss:

$$L_{\text{OR}}(\theta) = \mathbb{E}_{n_l} \mathcal{L}(\mathcal{G}_\theta(\mathbf{y}_l), \mathbf{z}_l) + \mathbb{E}_{n_u} \mathcal{L}(\mathcal{G}_\theta(\mathbf{y}_u), \hat{\mathcal{G}}(\mathbf{y}_u)) \quad (7)$$

which is also known as the Outcome Regression (OR) estimator of the loss in causal inference literature, *i.e.* we are *imputing* the missing label \mathbf{z}_u with the synthetic preference. However, this estimator is biased because the synthetic preference $\hat{\mathbf{z}}$ differs from the ground truth human preference \mathbf{z} in general. Alternatively, in this paper, we propose using the *debiased loss* as follows:

$$\begin{aligned} \mathcal{L}_{\text{DeDPO}}(\theta) &= \mathbb{E}_{n_l+n_u} \mathcal{L}(\mathcal{G}_\theta(\mathbf{y}), \hat{\mathcal{G}}(\mathbf{y})) \\ &+ \mathbb{E}_{n_l} (\mathcal{L}(\mathcal{G}_\theta(\mathbf{y}_l), \mathbf{z}_l) - \mathcal{L}(\mathcal{G}_\theta(\mathbf{y}_l), \hat{\mathcal{G}}(\mathbf{y}_l))) \end{aligned} \quad (8)$$

In the remaining part of this section, we’ll verify that our proposed debiased loss in Eq. (8) is unbiased and robust, describe how we generate synthetic preference by $\hat{\mathcal{G}}$ to train the diffusion model in practice, and theoretically show the convergence rate of the diffusion model θ (seen as an implicit classifier) is robust to the potentially slow rate of the synthetic preference model $\hat{\mathcal{G}}$.

4.1. Our DeDPO loss is unbiased

The first important property of the debiased loss is that it is an unbiased estimator of the population-level DPO loss Eq. (6) no matter whether the pseudo label $\hat{\mathcal{G}}(\mathbf{y})$ is correct or not.

Proposition 1. *The expectation of our proposed debiased loss in Eq. (8) is equal to the expectation of the original DPO loss in Eq. (4), i.e. L_{DeDPO} is unbiased:*

$$\mathbb{E}[L_{DeDPO}(\theta)] = \mathbb{E}[\mathcal{L}_{DPO}(\theta)] \quad (9)$$

Proof. Simply re-order the terms in Eq. (8) as:

$$\begin{aligned} L_{DeDPO}(\theta) &= \mathbb{E}_{n_l} \mathcal{L}(\mathcal{G}_\theta(\mathbf{y}_l), \mathbf{z}_l) \\ &+ \left[\mathbb{E}_{n_l+n_u} \mathcal{L}(\mathcal{G}_\theta(\mathbf{y}), \hat{\mathcal{G}}(\mathbf{y})) - \mathbb{E}_{n_l} \mathcal{L}(\mathcal{G}_\theta(\mathbf{y}_l), \hat{\mathcal{G}}(\mathbf{y}_l)) \right] \end{aligned} \quad (10)$$

Then, the expectation of the first term is the population-level DPO loss Eq. (6), and the expectation of the second term is 0 because both are unbiased estimators of $\mathbb{E}[\mathcal{L}(\mathcal{G}_\theta(\mathbf{y}), \hat{\mathcal{G}}(\mathbf{y}))]$. \square

This tells us that we can safely use the synthetic preference labels and still our loss is unbiased, which leads to bias-free learning. Moreover, when the synthetic labels are perfect i.e. $\hat{\mathcal{G}}(\mathbf{y}) = \mathbf{z}$, the debiased loss becomes $\mathbb{E}_{n_l+n_u} \mathcal{L}(\mathcal{G}_\theta(\mathbf{y}), \hat{\mathcal{G}}(\mathbf{y}))$, effectively utilizing all of the data, and when they are completely wrong, then asymptotically it becomes $\mathbb{E}_{n_l} \mathcal{L}(\mathcal{G}_\theta(\mathbf{y}_l), \mathbf{z}_l)$ i.e. only the labeled data is used.

4.2. Robustness against incorrect synthetic labels

We strive to give an intuitive explanation of how the debiased loss works. First, we combine the 3 loss terms into one with a new target label:

Proposition 2. *Our debiased loss is characterized by using pure pseudo-labels for unlabeled data and applying an amplified correction from pseudo-labels toward ground-truth labels for labeled data.*

$$L_{DeDPO}(\theta) = \mathbb{E}_{n_l+n_u} \mathcal{L}(\mathcal{G}_\theta(\mathbf{y}), \hat{\mathbf{w}}) \quad (11)$$

where:

$$\hat{\mathbf{w}} = \begin{cases} \hat{\mathcal{G}}(\mathbf{y}) & \text{if } \mathbf{y} \text{ is unlabeled} \\ \hat{\mathcal{G}}(\mathbf{y}) + \frac{n_l+n_u}{n_l} (\mathbf{z} - \hat{\mathcal{G}}(\mathbf{y})) & \text{if } \mathbf{y} \text{ is labeled as } \mathbf{z} \end{cases}$$

Please refer to the supplementary for the proof. Intuitively, for unlabeled data points, our loss simply uses the pseudo-labels as the supervision signal. For labeled data points, the loss introduces a correction term $\mathbf{z} - \hat{\mathcal{G}}(\mathbf{y})$ that moves the pseudo-label toward the true label, amplified by the importance weight $\frac{n_l+n_u}{n_l} \geq 1$, which reflects the

scarcity of labeled data. When the pseudo-label is already correct, this correction term vanishes and the loss reduces to standard supervised learning. When the pseudo-label is incorrect, the amplified correction not only fixes the error on the labeled point itself but also implicitly influences nearby unlabeled points, pushing them in the correct direction. Under a smoothness assumption on $\hat{\mathcal{G}}(\mathbf{y})$, the labeled point thus steers its local neighborhood toward the correct label.

The importance weight can also be instance-dependent, especially when the labeled and unlabeled data are from different distributions. However, we found little gain from using this variant, and in practice, we often *uniformly sample* data from a large initially unlabeled pool for high-quality labeling.

4.3. Synthetic preference labels

In this section, we consider 2 main ways to generate synthetic preference labels:

1. From the implicit reward margin induced by the current policy θ itself, i.e. self-training.
2. From a pretrained vision-language model (VLM).

As discussed before, we don't consider feedback from reward models that have been trained on a large dataset of preference pairs (like [20]) because we are in the label-sparse setting. The second method is straight forward and the synthetic labels are fixed once DPO starts. We discuss the first method in more detail.

Implicit reward margin as pseudo labels. Self-training style synthetic labels in image classification are generated by the classifier at the previous iteration $\hat{\theta}$. The synthetic preference model therefore is $\hat{\mathcal{G}}(\mathbf{y}) = \mathcal{G}_{\hat{\theta}}(\mathbf{y})$ i.e. the classifier in Eq. (5) with parameter $\hat{\theta}$. Specifically, following [51] the loss at each given input is:

$$\delta(\mathcal{G}_{\hat{\theta}}(\alpha_1(\mathbf{y}))) \mathcal{L}(\mathcal{G}_\theta(\alpha_2(\mathbf{y})), \text{round}(\mathcal{G}_{\hat{\theta}}(\alpha_3(\mathbf{y})))) \quad (12)$$

where $\alpha_1, \alpha_2, \alpha_3$ are augmentations of the input \mathbf{y} , respectively, round converts the soft sigmoid predictions to hard labels, and δ is a threshold function that zeros out the loss when $\mathcal{G}_{\hat{\theta}}(\alpha_1(\mathbf{y}))$ falls below a certain confidence threshold (when the pseudo prediction is close to 0.5). In our alignment setting, since augmentations applied to the original image \mathbf{x}_0 are not standard in image generation, we instead use the noisy images at different time steps t as the augmentations, preventing confirmation bias from the same input. This requires 2 additional forward passes of the diffusion model for each input. However, we also found that using no augmentations is already effective.

4.4. Fast convergence of DeDPO under slow convergence of the synthetic preference.

We now discuss the second theoretical property of our debiased loss which relates the speed of convergence of the

learning process with respect to the number of samples and the quality of the synthetic preference model $\hat{\mathcal{G}}$. Technically [70] articulates this property as convergence of the gradient of the debiased loss to a saddle point. We state an alternative convergence result in the excess risk in the spirit of [12]:

Theorem 1 (Informal). *Under certain regularity conditions, namely*

1. *the synthetic preference model $\hat{\mathcal{G}}$ is trained on data independent of that for DPO training of θ*
2. *both the diffusion model θ and the preference model $\hat{\mathcal{G}}$ are sufficiently smooth*
3. *θ belongs to a VC-subgraph class*

then with high probability, the model θ learned by our DeDPO loss satisfies:

$$\|\theta - \theta^*\|_2^2 \leq O\left(\frac{1}{n_l + n_u}\right) + O\left(\|\hat{\mathcal{G}} - \mathcal{G}^*\|_4^4\right) \quad (13)$$

where θ^* and \mathcal{G}^* are optimal versions of θ and $\hat{\mathcal{G}}$, and $\|\cdot\|_2$ and $\|\cdot\|_4$ are L_2 and L_4 norms: $\|f\|_2 = (\mathbb{E}[f(x)^2])^{1/2}$ and $\|f\|_4 = (\mathbb{E}[f(x)^4])^{1/4}$.

The proof and assumptions mostly follow [12]. The most exciting aspect of Theorem 1 is the 4th-power of right side’s second term $\|\hat{\mathcal{G}} - \mathcal{G}^*\|$, because it indicates that $\hat{\mathcal{G}}$ needs to converge only at a much slower rate $\frac{1}{(n_l + n_u)^{1/4}}$ for the target parameter θ to achieve the optimal convergence rate $\frac{1}{n_l + n_u}$. Therefore, our diffusion model can learn efficiently and robustly to the error in \mathcal{G} . Notably, the first assumption that the synthetic preference model $\hat{\mathcal{G}}$ is trained on an independent set of data from θ is violated by the self-training technique. This has practical consequences because if both θ and $\hat{\mathcal{G}}$ are trained on the labeled data, intuitively the correction terms in Proposition 2 will overfit to 0, providing no signal for correction. Therefore, pretrained vision–language models are the preferred choice, and our setting is well suited to them.

5. Experiments

5.1. Experimental setup

Datasets. For training, we use the FiFA dataset [65], a high-quality subset of human preference data filtered from the Pick-a-Pic v2 [23] and HPSv2 [60]. Following [65], we use the FiFA split containing 5K generated image pairs with human-labeled preferences, which was shown to outperform training on the full Pick-a-Pic v2 dataset. To study the semi-supervised setting with scarce human feedback, we partition FiFA into 25% labeled and 75% unlabeled pairs. The labeled subset is used with ground-truth human preferences, while the remaining 75% unlabeled

pairs are assigned synthetic preferences from an AI feedback¹. For evaluation, we follow standard text-to-image alignment benchmarks and use two prompt sets at test time: (i) PartiPrompt [67], which contains 1,632 diverse textual prompts, and (ii) the HPSv2 benchmark prompts [60], which consist of 4 categories with 800 prompts each, for a total of 3,200 prompts.

Evaluation protocols. We compare DeDPO against supervised fine-tuning (SFT) and Diffusion-DPO [57] using two backbone diffusion models: SD1.5 and SDXL. We use standard automatic preference metrics. On the PartiPrompt test set, we report PickScore [23] (PS) and Aesthetic Score² (AS), computed over images generated from all prompts. On the HPSv2 benchmark [60], we report the average HPSv2 score across its four categories, following the original protocol.

Implementation details. Training) We train on the 25% human-labeled and 75% pseudo-labeled FiFA-5K [65] and HPDv2 [60] split described above. For SD1.5, we fine-tune for 1,000 optimization steps using AdamW [32], a learning rate of 1×10^{-7} , a piecewise-constant learning rate schedule with 10 warmup steps, a global batch size of 128, 2 GPUs, and 8 gradient accumulation steps. For SDXL, we train for 100 steps using the AdaFactor [49] optimizer with a learning rate of 2×10^{-8} , 5 warmup steps, and the same piecewise-constant schedule. **Inference**) At test time, we sample images using 20 denoising steps with DDPM-Solver++ [33] as the noise scheduler and a classifier-free guidance (CFG) scale of 7.5 for all methods and backbones.

5.2. Results

Quantitative results. Table 1 shows that DeDPO with 25% human and 75% synthetic preferences is competitive with, and sometimes slightly better than, the fully supervised DPO baseline that uses 100% human labels. On FiFA-5K, DeDPO trained on SD1.5 even edges out DPO+100% in both PickScore and HPSv2 (21.91 vs. 21.88 PS; 27.80 vs. 27.79 HPSv2), and on SDXL it essentially matches the fully supervised model (22.83 vs. 22.84 PS with identical HPSv2). On HPDv2, DeDPO remains on par with DPO+100% for SD1.5 and slightly improves alignment for SDXL in both metrics, despite using only a quarter of the human annotations. More importantly, in our challenging semi-supervised setting, mixing human and synthetic labels with DPO consistently underperforms DeDPO under the same label budget. For example, on FiFA-5K, DPO with synthetic preferences is noticeably worse than DeDPO for both backbones (e.g., a gap of about 0.2 PickScore on SD1.5), and similar trends hold on HPDv2. This indicates that simply adding synthetic preferences can degrade

¹<https://huggingface.co/Qwen/Qwen2.5-VL-7B-Instruct>

²<https://github.com/christophschuhmann/improved-aesthetic-predictor>

Table 1. Main results for SD1.5 and SDXL trained on two preference datasets, FiFA-5K [65] and HPDv2 [60]. The best results are **bolded**, while the second-best results are underlined and zero un-preference pairs indicating using only ground truth preferences.

Training set	Model	Method	# Pref. pairs	# Unpref. pairs	PS [23] (↑)	HPSv2 Avg. [60] (↑)	AS (↑)
FiFA-5K [65]	SD1.5	SFT	1250	0	21.64	27.62	5.43
		DPO [57] + 25%	1250	0	21.76	27.76	<u>5.38</u>
		DPO [57] + 100%	5000	0	<u>21.88</u>	<u>27.79</u>	<u>5.38</u>
		DPO [57] + synthetic pref.	1250	3750	21.71	27.39	5.33
	SDXL	DeDPO + synthetic pref.	1250	3750	21.91	27.80	5.43
HPDv2 [60]	SD1.5	SFT	1250	0	22.01	27.87	5.60
		DPO [57] + 25%	1250	0	22.57	28.34	<u>5.66</u>
		DPO [57] + 100%	5000	0	22.84	28.76	5.77
		DPO [57] + synthetic pref.	1250	3750	22.61	<u>28.71</u>	<u>5.66</u>
	SDXL	DeDPO + synthetic pref.	1250	3750	<u>22.83</u>	28.76	5.77

alignment, whereas DeDPO is robust to these noises and can turn synthetic labels into a net gain relative to both semi-supervised DPO and the fully-supervised DPO upper bound.

Qualitative results. Fig. 1 compares SDXL samples from DeDPO trained with 25% human and 75% synthetic preferences (top row) to DPO trained with 25% human labels and to the fully supervised DPO model with 100% human labels. Across all four prompts, DeDPO better captures fine-grained details and compositional constraints. For example, in the “astronaut Lincoln” prompt, DeDPO renders a clear opaque helmet and a lunar setting, whereas others omit the helmet and has weaker space context. In the “I chased an elephant in my pajamas” and “carriage on the moon” prompts, DeDPO produces scenes that more faithfully reflect the described narrative and background elements (e.g., the movement context, the Statue of Liberty and pyramids), while DPO often simplifies or drops key components. For the steampunk pharaoh, DeDPO generates sharper styling cues such as the goggles and leather jacket. Overall, these examples illustrate that, even with substantially fewer human-labeled preferences, DeDPO attains or surpasses the visual quality and prompt adherence of DPO trained on the full high-quality dataset.

AI as a judge. To assess qualitative alignment, we adopt an AI-as-a-judge protocol following the human evaluation setup of Diffusion-DPO [57]. We use Gemini 2.5 Flash

as the judge: for each PartiPrompt [67] text prompt, we generate one image from each model, present the pair in random order, and ask the judge to pick a winner (or tie) along three criteria: *General Preference*, *Visual Appeal*, and *Prompt Alignment*, along with a short rationale. We run two SDXL comparisons on 200 randomly sampled prompts: (a) DeDPO (25% human, 75% synthetic) vs. fully supervised DPO (100% human), and (b) DeDPO vs. DPO under the same 25%/75% semi-supervised setting. As shown in Fig. 2, the judge prefers DeDPO over fully supervised DPO in most cases for General Preference and Visual Appeal (about 57% vs. 27–31% wins), with similar Prompt Alignment and many ties. Against semi-supervised DPO, the advantage is even clearer: DeDPO wins roughly 76–78% of comparisons in General Preference and Visual Appeal, and substantially more often in Prompt Alignment.

6. Ablation

Effect of synthetic preference sources. Tabs. 2 and 3 compare three sources of synthetic preferences: self-training, CLIP, and the multimodal LLM Qwen. Across both FiFA-5K and HPDv2, DeDPO is better than DPO and usually yields a small but consistent gain for each feedback source (e.g., on FiFA-5K with SDv1.5 and CLIP, PickScore improves from 21.46 to 21.90; with Qwen, from 21.71 to 21.91; on HPDv2 with SDXL and Qwen, from 22.52 to 22.55). The choice of feedback source also matters.

A statue of Abraham Lincoln wearing an opaque and shiny astronaut’s helmet. The statue sits on the moon, with the planet Earth in the sky.

One morning I chased an elephant in my pajamas

Horses pulling a carriage on the moon’s surface, with the Statue of Liberty and Great Pyramid in the background.

The Planet Earth can be seen in the sky.

A photograph of a portrait of a statue of a pharaoh wearing steampunk glasses, white t-shirt and leather jacket.



Figure 1. Our method achieves performance comparable to models trained on high-quality labels, particularly excelling at capturing subtle details within complex prompts. DeDPO successfully renders challenging elements like the astronaut helmet on Abraham Lincoln’s statue, the Statue of Liberty on the lunar carriage, and specific styling details in the pharaoh’s steampunk attire.

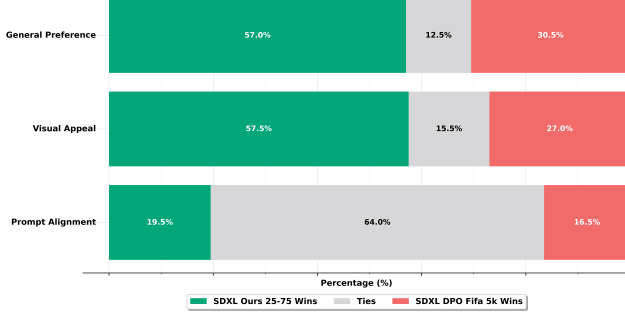
On both datasets, Qwen-based preferences generally give the best performance, particularly for SDXL on FiFA-5K (22.61 → 22.83), while CLIP and self-training are slightly weaker. This is consistent with a label-quality analysis on a held-out subset: Qwen’s pseudo labels agree with human preferences in just over approximately 80% of pairs, whereas CLIP matches only about 50% of the time, effectively behaving like a noisy guess.

Effect of training set size. Tab. 4 examines how performance changes as we scale the total number of training pairs while keeping the labeled–unlabeled ratio fixed at 25%–75%. Here, we train SD1.5 and report PickScore on

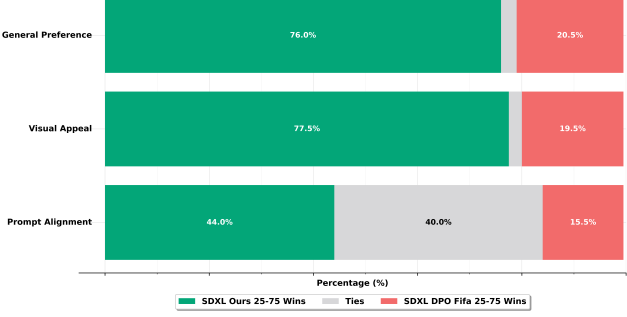
Table 2. Effect of different synthetic preference sources in FiFA-5K.

Model	Method	Self-Training [70]	CLIP[40]	Qwen [55]
SDv1.5	DPO [57]	21.79	21.46	21.71
SDv1.5	DeDPO	21.84	21.90	21.91
SDXL	DPO [57]	22.60	22.50	22.61
SDXL	DeDPO	22.62	22.57	22.83

the PartiPrompt benchmark. Across all sizes, DeDPO consistently outperforms DPO by roughly 0.1–0.2 PickScore



(a) DeDPO vs. DPO (100% human).



(b) DeDPO vs. DPO (25% human - 75% synthetic).

Figure 2. AI-as-a-judge comparison on 200 PartiPrompt prompts [67]. Gemini 2.5 Flash evaluates each image pair on General Preference, Visual Appeal, and Prompt Alignment. The judge can cast either a win or a tie vote for the image pair.

Table 3. Effect of different synthetic preference sources in HPDv2.

Model	Method	Self-Training [70]	CLIP[40]	Qwen [55]
SDv1.5	DPO [57]	21.60	21.53	21.69
SDv1.5	DeDPO	21.65	21.60	21.66
SDXL	DPO [57]	22.50	22.45	22.52
SDXL	DeDPO	22.52	22.44	22.55

and already achieves 21.9x at the smallest 5K setting. For DPO, performance improves only slightly from 5K to 20K (21.71 \rightarrow 21.79) and then saturates or even drops at 50K and 100K, whereas DeDPO remains stable. A plausible explanation, consistent with FiFA [65], is that enlarging the dataset brings in proportionally more noisy preferences from Pick-a-Pic-v2; DPO is more sensitive to this noise, while DeDPO is more robust.

Table 4. Effect of training set size when keeping the ratio labeled-unlabeled at 25%-75%

Method	5K	10K	20K	50K	100K
DPO [57]	21.71	21.76	21.79	21.76	21.7
DeDPO	21.91	21.86	21.87	21.85	21.87

Effect of unlabeled data size. In Fig. 3 we fix the number of human-labeled pairs to 1.2K and vary the amount of synthetically-labeled unlabeled data when training SD1.5, evaluating PickScore on PartiPrompt. DeDPO consistently outperforms vanilla DPO for all unlabeled sizes, with a gap of roughly 0.1–0.2 PickScore. For DPO, performance peaks at a moderate amount of unlabeled data (8K: 21.82) but then degrades as we add more synthetic pairs (down to 21.70 at 38K and 21.69 at 98K), indicating that large quantities of noisy synthetic labels can hurt alignment. In contrast, DeDPO’s performance remains stable as the number of unlabeled samples scales: it marginally improves from 21.91

to 21.96 (38K samples) and sees only a minimal reduction to 21.89 (98K samples). Throughout this scaling, DeDPO consistently outperforms all DPO variants.

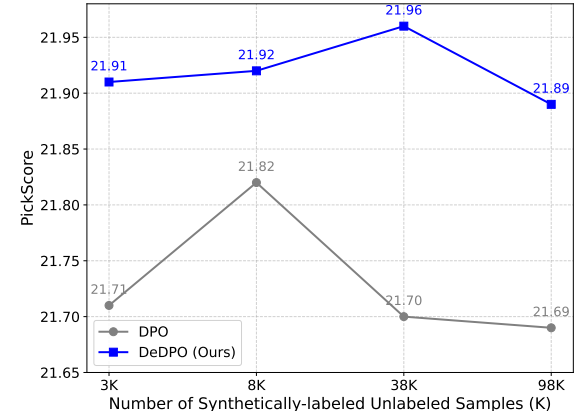


Figure 3. Ablation on the size of the unlabeled data set. We fix the labeled data size to 1.2K pairs and vary the number of unlabeled pairs to 3K, 8K, 38K and 98K. DeDPO clearly show superior results across varying unlabeled data set size.

7. Conclusion & Discussion

In this work, we address the scalability bottleneck of preference optimization by proposing Debiased DPO (DeDPO). Motivated by the prohibitive cost of human supervision, DeDPO integrates a debiased estimation method from causal inference to robustly leverage large volumes of inexpensive, yet noisy, synthetic preference labels. Empirical results across multiple diffusion models and synthetic annotators demonstrate that DeDPO significantly outperforms naive synthetic training and matches or exceeds models trained on fully human-labeled data. Consequently, our approach facilitates scalable human-AI alignment, proving that properly debiased synthetic feedback is a reliable and cost-effective surrogate for extensive human labeling.

References

[1] Mohammad Gheshlaghi Azar, Zhaohan Daniel Guo, Bilal Piot, Remi Munos, Mark Rowland, Michal Valko, and Daniele Calandriello. A general theoretical paradigm to understand learning from human preferences. In *International Conference on Artificial Intelligence and Statistics*, pages 4447–4455. PMLR, 2024. 3

[2] Heejung Bang and James M. Robins. Doubly robust estimation in missing data and causal inference models. *Biometrics*, 61(4):962–973, 2005. 2

[3] Kevin Black, Michael Janner, Yilun Du, Ilya Kostrikov, and Sergey Levine. Training diffusion models with reinforcement learning. *arXiv preprint arXiv:2305.13301*, 2023. 1

[4] Alexander Bukharin, Ilgee Hong, Haoming Jiang, Zichong Li, Qingru Zhang, Zixuan Zhang, and Tuo Zhao. Robust reinforcement learning from corrupted human feedback. *Advances in Neural Information Processing Systems*, 37: 124093–124113, 2024. 2

[5] Souradip Chakraborty, Jiahao Qiu, Hui Yuan, Alec Koppel, Furong Huang, Dinesh Manocha, Amrit Singh Bedi, and Mengdi Wang. Maxmin-rlhf: Alignment with diverse human preferences. *arXiv preprint arXiv:2402.08925*, 2024. 2

[6] Victor Chernozhukov, Denis Chetverikov, Mert Demirer, Esther Duflo, Christian Hansen, Whitney Newey, and James Robins. Double/debiased machine learning for treatment and structural parameters, 2018. 2

[7] Sayak Ray Chowdhury, Anush Kini, and Nagarajan Natarajan. Provably robust dpo: Aligning language models with noisy feedback. *arXiv preprint arXiv:2403.00409*, 2024. 2, 1

[8] Yihe Deng, Pan Lu, Fan Yin, Ziniu Hu, Sheng Shen, Quanquan Gu, James Y Zou, Kai-Wei Chang, and Wei Wang. Enhancing large vision language models with self-training on image comprehension. *Advances in Neural Information Processing Systems*, 37:131369–131397, 2024. 2

[9] Prafulla Dhariwal and Alexander Nichol. Diffusion models beat gans on image synthesis. *Advances in neural information processing systems*, 34:8780–8794, 2021. 1, 2, 3

[10] Miroslav Dudík, Dumitru Erhan, John Langford, and Lihong Li. Doubly robust policy evaluation and optimization. *Statistical Science*, 29(4):485–511, 2014. 2

[11] Ying Fan, Olivia Watkins, Yuqing Du, Hao Liu, Moonkyung Ryu, Craig Boutilier, Pieter Abbeel, Mohammad Ghavamzadeh, Kangwook Lee, and Kimin Lee. Dpok: Reinforcement learning for fine-tuning text-to-image diffusion models. *Advances in Neural Information Processing Systems*, 36:79858–79885, 2023. 1

[12] Dylan J Foster and Vasilis Syrgkanis. Orthogonal statistical learning. *The Annals of Statistics*, 51(3):879–908, 2023. 2, 5, 1

[13] Jiayi Fu, Xuandong Zhao, Chengyuan Yao, Heng Wang, Qi Han, and Yanghua Xiao. Reward shaping to mitigate reward hacking in rlhf. *arXiv preprint arXiv:2502.18770*, 2025. 2

[14] Shangmin Guo, Biao Zhang, Tianlin Liu, Tianqi Liu, Misha Khalman, Felipe Llinares, Alexandre Rame, Thomas Mesnard, Yao Zhao, Bilal Piot, et al. Direct language model alignment from online ai feedback. *arXiv preprint arXiv:2402.04792*, 2024. 1

[15] Cheng-Ju Ho, Chen-Hsuan Tai, Yen-Yu Lin, Ming-Hsuan Yang, and Yi-Hsuan Tsai. Diffusion-ss3d: Diffusion model for semi-supervised 3d object detection. *Advances in Neural Information Processing Systems*, 36:49100–49112, 2023. 1

[16] Jonathan Ho and Tim Salimans. Classifier-free diffusion guidance. *arXiv preprint arXiv:2207.12598*, 2022. 3

[17] Jonathan Ho, Ajay Jain, and Pieter Abbeel. Denoising diffusion probabilistic models. *Advances in neural information processing systems*, 33:6840–6851, 2020. 2

[18] Aaron Jaech, Adam Kalai, Adam Lerer, Adam Richardson, Ahmed El-Kishky, Aiden Low, Alec Helyar, Aleksander Madry, Alex Beutel, Alex Carney, et al. Openai o1 system card. *arXiv preprint arXiv:2412.16720*, 2024. 1

[19] Nan Jiang and Lihong Li. Doubly robust off-policy evaluation for reinforcement learning. In *Proc. of the 33rd Int'l Conf. on Machine Learning (ICML)*, pages 652–661, 2016. 2

[20] Shyamgopal Karthik, Huseyin Coskun, Zeynep Akata, Sergey Tulyakov, Jian Ren, and Anil Kag. Scalable ranked preference optimization for text-to-image generation. In *Proceedings of the IEEE/CVF International Conference on Computer Vision*, pages 18399–18410, 2025. 2, 4

[21] Edward H Kennedy. Semiparametric doubly robust targeted double machine learning: a review. *Handbook of statistical methods for precision medicine*, pages 207–236, 2024. 2

[22] Cheol Woo Kim, Shresth Verma, Mauricio Tec, and Milind Tambe. Lightweight robust direct preference optimization. *arXiv preprint arXiv:2510.23590*, 2025. 2

[23] Yuval Kirstain, Adam Polyak, Uriel Singer, Shahbuland Matiana, Joe Penna, and Omer Levy. Pick-a-pic: An open dataset of user preferences for text-to-image generation, 2023. 5, 6

[24] Yuval Kirstain, Adam Polyak, Uriel Singer, Shahbuland Matiana, Joe Penna, and Omer Levy. Pick-a-pic: An open dataset of user preferences for text-to-image generation. *Advances in neural information processing systems*, 36:36652–36663, 2023. 2

[25] Harrison Lee, Samrat Phatale, Hassan Mansoor, Thomas Mesnard, Johan Ferret, Kellie Lu, Colton Bishop, Ethan Hall, Victor Carbune, Abhinav Rastogi, and Sushant Prakash. Rlaif vs. rlhf: Scaling reinforcement learning from human feedback with ai feedback. In *Proceedings of the 41st International Conference on Machine Learning (ICML)*, 2024. 1

[26] Chunyuan Li, Cliff Wong, Sheng Zhang, Naoto Usuyama, Haotian Liu, Jianwei Yang, Tristan Naumann, Hoifung Poon, and Jianfeng Gao. Llava-med: Training a large language-and-vision assistant for biomedicine in one day. *Advances in Neural Information Processing Systems*, 36:28541–28564, 2023. 2

[27] Huayang Li, Siheng Li, Deng Cai, Longyue Wang, Lemao Liu, Taro Watanabe, Yujiu Yang, and Shuming Shi. Textbind: Multi-turn interleaved multimodal instruction-following in the wild. In *Findings of the Association for Computational Linguistics: ACL 2024*, pages 9053–9076, 2024.

[28] Lei Li, Zhihui Xie, Mukai Li, Shunian Chen, Peiyi Wang, Liang Chen, Yazheng Yang, Benyou Wang, Lingpeng Kong, and Qi Liu. Vlfeedback: A large-scale ai feedback dataset for large vision-language models alignment. *arXiv preprint arXiv:2410.09421*, 2024. 2

[29] Ruining Li, Chuanxia Zheng, Christian Rupprecht, and Andrea Vedaldi. Dso: Aligning 3d generators with simulation feedback for physical soundness. In *ICCV*, 2025. 1

[30] Haotian Liu, Chunyuan Li, Qingyang Wu, and Yong Jae Lee. Visual instruction tuning. *Advances in neural information processing systems*, 36:34892–34916, 2023. 2

[31] Jie Liu, Gongye Liu, Jiajun Liang, Ziyang Yuan, Xiaokun Liu, Mingwu Zheng, Xiele Wu, Qiulin Wang, Menghan Xia, Xintao Wang, et al. Improving video generation with human feedback. *arXiv preprint arXiv:2501.13918*, 2025. 1

[32] I Loshchilov. Decoupled weight decay regularization. *arXiv preprint arXiv:1711.05101*, 2017. 5

[33] Cheng Lu, Yuhao Zhou, Fan Bao, Jianfei Chen, Chongxuan Li, and Jun Zhu. Dpm-solver++: Fast solver for guided sampling of diffusion probabilistic models. *Machine Intelligence Research*, pages 1–22, 2025. 5

[34] Debmalya Mandal, Paulius Sasnauskas, and Goran Radanovic. Distributionally robust reinforcement learning with human feedback. *arXiv preprint arXiv:2503.00539*, 2025. 2

[35] Eric Mitchell. A note on dpo with noisy preferences and relationship to ipo, 2023. URL <https://ericmitchell.ai/cdpo.pdf>, 2023. 2, 1, 3

[36] Volodymyr Mnih, Adria Puigdomenech Badia, Mehdi Mirza, Alex Graves, Timothy Lillicrap, Tim Harley, David Silver, and Koray Kavukcuoglu. Asynchronous methods for deep reinforcement learning. In *International conference on machine learning*, pages 1928–1937. PMLR, 2016. 1

[37] Long Ouyang, Jeffrey Wu, Xu Jiang, Diogo Almeida, Carroll Wainwright, Pamela Mishkin, Chong Zhang, Sandhini Agarwal, Katarina Slama, Alex Ray, et al. Training language models to follow instructions with human feedback. *Advances in neural information processing systems*, 35:27730–27744, 2022. 1

[38] Vishakh Padmakumar, Chuanyang Jin, Hannah Rose Kirk, and He He. Beyond the binary: Capturing diverse preferences with reward regularization. *arXiv preprint arXiv:2412.03822*, 2024. 2

[39] Liang Peng, Boxi Wu, Haoran Cheng, Yibo Zhao, and Xiaofei He. Self-supervised direct preference optimization for text-to-image diffusion models. In *The Thirty-ninth Annual Conference on Neural Information Processing Systems*, 2025. 1

[40] Alec Radford, Jong Wook Kim, Chris Hallacy, Aditya Ramesh, Gabriel Goh, Sandhini Agarwal, Girish Sastry, Amanda Askell, Pamela Mishkin, Jack Clark, et al. Learning transferable visual models from natural language supervision. In *International conference on machine learning*, pages 8748–8763. PMLR, 2021. 7, 8

[41] Alec Radford, Jong Wook Kim, Chris Hallacy, Aditya Ramesh, Gabriel Goh, Sandhini Agarwal, Girish Sastry, Amanda Askell, Pamela Mishkin, Jack Clark, et al. Learning transferable visual models from natural language supervision. In *International conference on machine learning*, pages 8748–8763. PMLR, 2021. 2

[42] Rafael Rafailov, Archit Sharma, Eric Mitchell, Christopher D Manning, Stefano Ermon, and Chelsea Finn. Direct preference optimization: Your language model is secretly a reward model. *Advances in neural information processing systems*, 36:53728–53741, 2023. 1, 3

[43] James M. Robins, Andrea Rotnitzky, and Lue Ping Zhao. Estimation of regression coefficients when some regressors are not always observed. *Journal of the American Statistical Association*, 89(427):846–866, 1994. 2

[44] Robin Rombach, Andreas Blattmann, Dominik Lorenz, Patrick Esser, and Björn Ommer. High-resolution image synthesis with latent diffusion models. In *Proceedings of the IEEE/CVF conference on computer vision and pattern recognition*, pages 10684–10695, 2022. 1, 2

[45] Daniel O. Scharfstein, Andrea Rotnitzky, and James M. Robins. Adjusting for nonignorable drop-out using semiparametric nonresponse models. *Journal of the American Statistical Association*, 94(448):1096–1120, 1999. 2

[46] Christoph Schuhmann. Laion-aesthetics, 2022. Accessed: 2023-11-10. 2

[47] Christoph Schuhmann, Romain Beaumont, Richard Vencu, Cade Gordon, Ross Wightman, Mehdi Cherti, Theo Coombes, Aarush Katta, Clayton Mullis, Mitchell Wortsman, et al. Laion-5b: An open large-scale dataset for training next generation image-text models. *Advances in Neural Information Processing Systems*, 35:25278–25294, 2022. 1

[48] John Schulman, Filip Wolski, Prafulla Dhariwal, Alec Radford, and Oleg Klimov. Proximal policy optimization algorithms. *arXiv preprint arXiv:1707.06347*, 2017. 1

[49] Noam Shazeer and Mitchell Stern. Adafactor: Adaptive learning rates with sublinear memory cost. In *International Conference on Machine Learning*, pages 4596–4604. PMLR, 2018. 5

[50] Yutao Shen, Junkun Yuan, Toru Aonishi, Hideki Nakayama, and Yue Ma. Follow-your-preference: Towards preference-aligned image inpainting. *arXiv preprint arXiv:2509.23082*, 2025. 1

[51] Kihyuk Sohn, David Berthelot, Nicholas Carlini, Zizhao Zhang, Han Zhang, Colin A Raffel, Ekin Dogus Cubuk, Alexey Kurakin, and Chun-Liang Li. Fixmatch: Simplifying semi-supervised learning with consistency and confidence. *Advances in neural information processing systems*, 33:596–608, 2020. 4

[52] Jiaming Song, Chenlin Meng, and Stefano Ermon. Denoising diffusion implicit models. *arXiv preprint arXiv:2010.02502*, 2020. 2

[53] Yang Song, Jascha Sohl-Dickstein, Diederik P Kingma, Abhishek Kumar, Stefano Ermon, and Ben Poole. Score-based generative modeling through stochastic differential equations. *arXiv preprint arXiv:2011.13456*, 2020. 2

[54] Christian Szegedy, Vincent Vanhoucke, Sergey Ioffe, Jon Shlens, and Zbigniew Wojna. Rethinking the inception architecture for computer vision. In *Proceedings of the IEEE conference on computer vision and pattern recognition*, pages 2818–2826, 2016. 2

[55] Qwen Team. Qwen2.5-vl, 2025. 7, 8

[56] Philip S. Thomas and Emma Brunskill. Data-efficient off-policy policy evaluation for reinforcement learning. In *Proc. of the 33rd Int'l Conf. on Machine Learning (ICML)*, pages 2139–2148, 2016. 2

[57] Bram Wallace, Meihua Dang, Rafael Rafailov, Linqi Zhou, Aaron Lou, Senthil Purushwalkam, Stefano Ermon, Caiming Xiong, Shafiq Joty, and Nikhil Naik. Diffusion model alignment using direct preference optimization. In *Proceedings of the IEEE/CVF Conference on Computer Vision and Pattern Recognition*, pages 8228–8238, 2024. 1, 2, 3, 5, 6, 7, 8

[58] Junke Wang, Lingchen Meng, Zejia Weng, Bo He, Zuxuan Wu, and Yu-Gang Jiang. To see is to believe: Prompting gpt-4v for better visual instruction tuning. *arXiv preprint arXiv:2311.07574*, 2023. 2

[59] Junkang Wu, Yuexiang Xie, Zhengyi Yang, Jiancan Wu, Ji-awei Chen, Jinyang Gao, Bolin Ding, Xiang Wang, and Xi-angnan He. Towards robust alignment of language models: Distributionally robustifying direct preference optimization. *arXiv preprint arXiv:2407.07880*, 2024. 2, 1, 3

[60] Xiaoshi Wu, Keqiang Sun, Feng Zhu, Rui Zhao, and Hongsheng Li. Human preference score: Better aligning text-to-image models with human preference. In *Proceedings of the IEEE/CVF International Conference on Computer Vision*, pages 2096–2105, 2023. 2, 5, 6, 3

[61] Ziyi Wu, Anil Kag, Ivan Skorokhodov, Willi Menapace, Ashkan Mirzaei, Igor Gilitschenski, Sergey Tulyakov, and Aliaksandr Siarohin. Densedpo: Fine-grained temporal preference optimization for video diffusion models. *arXiv preprint arXiv:2506.03517*, 2025. 1

[62] Erhan Xu, Kai Ye, Hongyi Zhou, Luhuan Zhu, Francesco Quinza, and Chengchun Shi. Doubly robust alignment for large language models. *Advances in Neural Information Processing Systems (NeurIPS)*, 2025. to appear, also available as *arXiv:2506.01183*. 2

[63] Zaiyan Xu, Sushil Vemuri, Kishan Panaganti, Dileep Kalathil, Rahul Jain, and Deepak Ramachandran. Robust llm alignment via distributionally robust direct preference optimization. *arXiv preprint arXiv:2502.01930*, 2025. 2, 1

[64] Yuzi Yan, Xingzhou Lou, Jialian Li, Yiping Zhang, Jian Xie, Chao Yu, Yu Wang, Dong Yan, and Yuan Shen. Reward-robust rlhf in llms. *arXiv preprint arXiv:2409.15360*, 2024. 2

[65] Yongjin Yang, Sihyeon Kim, Hojung Jung, Sangmin Bae, SangMook Kim, Se-Young Yun, and Kimin Lee. Automated filtering of human feedback data for aligning text-to-image diffusion models. *arXiv preprint arXiv:2410.10166*, 2024. 5, 6, 8

[66] Kai Ye, Hongyi Zhou, Jin Zhu, Francesco Quinza, and Chengchun Shi. Robust reinforcement learning from human feedback for large language models fine-tuning. *arXiv preprint arXiv:2504.03784*, 2025. 2

[67] Jiahui Yu, Yuanzhong Xu, Jing Yu Koh, Thang Luong, Gunjan Baid, Zirui Wang, Vijay Vasudevan, Alexander Ku, Yinfei Yang, Burcu Karagol Ayan, et al. Scaling autoregressive models for content-rich text-to-image generation. *arXiv preprint arXiv:2206.10789*, 2(3):5, 2022. 5, 6, 8

[68] Huizhuo Yuan, Zixiang Chen, Kaixuan Ji, and Quanquan Gu. Self-play fine-tuning of diffusion models for text-to-image generation. *Advances in Neural Information Processing Systems*, 37:73366–73398, 2024. 2

[69] Yanzhe Zhang, Ruiyi Zhang, Jiuxiang Gu, Yufan Zhou, Nedim Lipka, Diyi Yang, and Tong Sun. Llavar: Enhanced visual instruction tuning for text-rich image understanding. *arXiv preprint arXiv:2306.17107*, 2023. 2

[70] Banghua Zhu, Mingyu Ding, Philip Jacobson, Ming Wu, Wei Zhan, Michael Jordan, and Jiantao Jiao. Doubly-robust self-training. *Advances in Neural Information Processing Systems*, 36:41413–41431, 2023. 2, 5, 7, 8, 1

DeDPO: Debiased Direct Preference Optimization for Diffusion Models

Supplementary Material

In this supplementary materials, we provide additional quantitative and qualitative evidences, along with formal theoretical proofs, to further support our work on DeDPO.

DeDPO

Further discussion on related works. As noted in the related work section, our method is different from other existing robustness works. In particular Chowdhury et al. [7], Mitchell [35] assume that the flip rate is known, while Wu et al. [59], Xu et al. [63] use distributionally robust optimization to guard against the worst-case scenario. Comparing to the former, our setting is far from random flip, as synthetic feedback from other models will have clear error patterns rather than randomly wrong guesses. Comparing to the later, we can beat the worst base thanks to the labeled dataset correcting the error patterns made by the label models. We show this comparison in paragraph 7. Secondly, [70] is a closely related work that applies the same debiased loss to image classification. However, a crucial difference is that they instantiate the framework with self-training only, where synthetic classification labels are taken from the same model. Self-training violates the Assumption 1, also known as sample splitting or cross-fitting, required for Theorem 1 to work for a flexible class of models. Intuitively, if we train a preference model on the same set of labeled data to create synthetic preference labels for the rest of the dataset, we effectively overfit on this labeled dataset, resulting in no correction in Proposition 2 and so all labels collapse to \hat{G} , making the second training vacuous. Theoretically, we can satisfy Assumption 1 by dividing the labeled dataset into 2, use the first set to train \hat{G} and synthetically label the unlabeled data, then use the second set to train θ . This works in theory because asymptotically there is no difference between n and $n/2$, but in practice it leads to significant degradation on the quality of both \hat{G} and θ , especially in our label-sparse setting. Besides, we also emphasize that we are the first robust DPO work in the generative vision domain, as all previously mentioned robust works are either in the language domain, or as classification in the vision domain.

Theoretical Proofs

Proof of Proposition 2.

Proof. First, we rewrite the second term of Eq. (8):

$$\begin{aligned} L_{\text{DeDPO}}(\theta) &= \mathbb{E}_{n_l+n_u} \mathcal{L}(\mathcal{G}_\theta(\mathbf{y}), \hat{\mathcal{G}}(\mathbf{y})) \\ &+ \mathbb{E}_{n_l} (\mathcal{L}(\mathcal{G}_\theta(\mathbf{y}_l), \mathbf{z}_l) - \mathcal{L}(\mathcal{G}_\theta(\mathbf{y}_l), \hat{\mathcal{G}}(\mathbf{y}_l))) \\ &= \mathbb{E}_{n_l+n_u} \mathcal{L}(\mathcal{G}_\theta(\mathbf{y}), \hat{\mathcal{G}}(\mathbf{y})) \\ &+ \mathbb{E}_{n_l+n_u} \frac{n_l + n_u}{n_l} \mathbf{r} (\mathcal{L}(\mathcal{G}_\theta(\mathbf{y}), \mathbf{z}) - \mathcal{L}(\mathcal{G}_\theta(\mathbf{y}), \hat{\mathcal{G}}(\mathbf{y}))) \end{aligned} \quad (14)$$

where \mathbf{r} is a binary variable which is 1 if \mathbf{y} is labeled and 0 otherwise. Second, we note that the binary cross-entropy loss is linear in the second argument i.e. the target label. Therefore, now that all terms share the same prediction $\mathcal{G}_\theta(\mathbf{y})$, we can add, subtract, and multiply the targets with the weight $\frac{n_l + n_u}{n_l} \mathbf{r}$ to get:

$$\begin{aligned} L_{\text{DeDPO}}(\theta) &= \\ \mathbb{E}_{n_l+n_u} \mathcal{L} \left(\mathcal{G}_\theta(\mathbf{y}), \hat{\mathcal{G}}(\mathbf{y}) + \frac{n_l + n_u}{n_l} \mathbf{r} (\mathbf{z} - \hat{\mathcal{G}}(\mathbf{y})) \right) & (15) \\ &= \mathbb{E}_{n_l+n_u} \mathcal{L}(\mathcal{G}_\theta(\mathbf{y}), \hat{\mathbf{w}}) \end{aligned}$$

for $\hat{\mathbf{w}}$ defined in the original claim. \square

Proof of Theorem 1. To state the theorem formally, we need several pre-processing steps. First, we change notations and use $\theta(\mathbf{y})$ to mean the logits in Eq. (4) as a function of the input \mathbf{y} , repeated here for convenience:

$$\theta(\mathbf{y}) = \left(-\beta (\|\boldsymbol{\epsilon}^w - \boldsymbol{\epsilon}_\theta(\mathbf{x}_t^w, t)\|_2^2 - \|\boldsymbol{\epsilon}^w - \boldsymbol{\epsilon}_{\text{ref}}(\mathbf{x}_t^w, t)\|_2^2 \right. \\ \left. - \|\boldsymbol{\epsilon}^l - \boldsymbol{\epsilon}_\theta(\mathbf{x}_t^l, t)\|_2^2 + \|\boldsymbol{\epsilon}^l - \boldsymbol{\epsilon}_{\text{ref}}(\mathbf{x}_t^l, t)\|_2^2) \right)$$

and $g(\mathbf{y})$ to mean the synthetic preference function as a function of the input \mathbf{y} , replacing $\hat{\mathcal{G}}(\mathbf{y})$ in the original claim. These changes are to make our claim more consistent with [12]. In addition, we introduce $\gamma(\mathbf{y})$ to mean the importance weight as a function of the input \mathbf{y} . While we have assumed that the importance weight is known and constant i.e. $\gamma(\mathbf{y}) = \frac{n_l + n_u}{n_l} \mathbf{r}$, we aim to state the theorem for the general case where $\gamma(\mathbf{y})$ is unknown and must be estimated and the sampling depends on the input covariate \mathbf{y} . While we use θ to denote the general function, we also use $\hat{\theta}$, θ^* to denote the learned and the optimal functions, respectively. We do the same for g and \hat{g} . Thus, Eq. (13) of the theorem is now:

$$\|\hat{\theta} - \theta^*\|_2^2 \leq O(1/n) + O(\|\hat{g} - g^*\|_4^4) \quad (16)$$

Therefore, we are bounding the difference between *outputs* of the learned $\hat{\theta}$ and the optimal θ^* in the L_2 norm. We also

write our population-level loss as

$$\begin{aligned} L(\theta, g, \gamma) &= \mathbb{E}[L_{\text{DeDPO}}(\theta, g, \gamma)] \\ &= \mathbb{E}[\mathcal{L}(\theta(\mathbf{y}), g(\mathbf{y}) + \gamma(\mathbf{y})(\mathbf{z} - g(\mathbf{y})))] \quad (17) \\ &= \mathbb{E}[\mathcal{L}(\theta(\mathbf{y}), w(g, \gamma)(\mathbf{y}))] \end{aligned}$$

i.e. a functional of θ, g and γ .

We next state the technical assumptions needed:

Assumption 1. $\hat{g}(\mathbf{y})$ is trained on data independent of that of $\theta(\mathbf{y})$.

Assumption 2. the logits $\theta(\mathbf{y})$ is bounded in $[-M, M]$ for all \mathbf{y} and constant M .

Assumption 3. The propensity estimate converges at least as fast as the preference estimate i.e. $\|\gamma - \gamma^*\|_4 \leq \|\hat{g} - g^*\|_4$

Assumption 4. The logits $\theta(\mathbf{y})$ belongs to a VC-subgraph class of bounded VC-dimension d . This means that empirical risk minimization of θ achieves fast convergence rate with respect to the population risk. Specifically, with probability at least $1 - \delta$, the following inequality holds:

$$\text{Rate} \leq C \frac{d \log n + \log(1/\delta)}{n} = O(d/n)$$

Recall the binary cross-entropy loss with logits a and target b :

$$\mathcal{L}(a, b) = -b \log \sigma(a) + (1 - b) \log(1 - \sigma(a)) \quad (18)$$

and the directional derivative of a functional L of f in the direction of another function f' is:

$$D_f L(f)[f - f'] = \frac{d}{dt} L(f + t(f - f')) \Big|_{t=0} \quad (19)$$

Before proceeding to the proof, we need the following lemma, which concerns the strong convexity of the loss \mathcal{L} with respect to θ :

Lemma 1 (Strong convexity). *For any θ, θ' , the following strong convexity inequality holds:*

$$\begin{aligned} D_\theta L(\theta, g, \gamma)[\theta - \theta'] - D_\theta L(\theta', g, \gamma)[\theta - \theta'] \\ \geq \lambda \|\theta - \theta'\|_2^2 \end{aligned} \quad (20)$$

where $\lambda = \sigma(M)(1 - \sigma(M))$ is a constant by Assumption 2.

Proof. The derivative of the point-wise binary cross-entropy loss $\mathcal{L}(\theta, g, \gamma)$ with respect to θ is:

$$\partial_\theta \mathcal{L}(\theta, g, \gamma) = \sigma(\theta(\mathbf{y})) - w(\mathbf{y}, \mathbf{z}) \quad (21)$$

and the second derivative is:

$$\partial_\theta^2 \mathcal{L}(\theta, g, \gamma) = \sigma(\theta(\mathbf{y}))(1 - \sigma(\theta(\mathbf{y}))) \quad (22)$$

(note the second derivative does not depend on w). σ is the sigmoid function. The expectation of the right-hand side achieves the minimum at the boundary, therefore by Assumption 2, it is at least λ i.e. the curvature of the point-wise \mathcal{L} is bounded below by λ .

Now, by the fundamental theorem of calculus, the difference in gradients as required by the lemma is the integral of the Hessian i.e. let $\theta_t = \theta + t(\theta - \theta')$ for $t \in [0, 1]$:

$$\begin{aligned} &D_\theta L(\theta, g, \gamma)[\theta - \theta'] - D_\theta L(\theta', g, \gamma)[\theta - \theta'] \\ &= \int_0^1 \partial_t D_\theta L(\theta_t, g, \gamma) dt \\ &= \int_0^1 D_\theta^2 L(\theta_t, g, \gamma)[\theta - \theta'] dt \\ &= \int_0^1 \mathbb{E} \partial_\theta^2 \mathcal{L}(\theta_t, g, \gamma)(\theta - \theta')^2 dt \\ &\geq \lambda \|\theta - \theta'\|_2^2 \end{aligned} \quad (23)$$

□

Now we are ready for the main proof. First we use Lemma 1 for the estimated and optimal logits $\hat{\theta}$ and θ^* :

$$D_\theta L(\hat{\theta}, \hat{g}, \hat{\gamma})[\hat{\theta} - \theta^*] - D_\theta L(\theta^*, \hat{g}, \hat{\gamma})[\hat{\theta} - \theta^*] \geq \lambda \|\hat{\theta} - \theta^*\|_2^2 \quad (24)$$

since $\hat{\theta}$ is the minimizer of $L(\hat{\theta}, \hat{g}, \hat{\gamma})$, we have $D_\theta L(\hat{\theta}, \hat{g}, \hat{\gamma})[\hat{\theta} - \theta^*] = 0$. Therefore, we get:

$$\begin{aligned} \lambda \|\hat{\theta} - \theta^*\|_2^2 &\leq -D_\theta L(\theta^*, \hat{g}, \hat{\gamma})[\hat{\theta} - \theta^*] \\ &= -\mathbb{E}[(\sigma(\theta^*(\mathbf{y})) - w(\hat{g}, \hat{\gamma})(\mathbf{y}, \mathbf{z}))(\hat{\theta}(\mathbf{y}) - \theta^*(\mathbf{y}))] \end{aligned} \quad (25)$$

using that $D_\theta L(\theta^*, g^*, \gamma^*)[\hat{\theta} - \theta^*] = 0$ due to optimality of θ^* , and also that $D_\theta L(\theta^*, g^*, \gamma^*)[\hat{\theta} - \theta^*] = \mathbb{E}[\sigma(\theta^*) - w(g^*, \gamma^*)](\hat{\theta} - \theta^*)$ by simple differentiation, we add $0 = \mathbb{E}[\sigma(\theta^*) - w(g^*, \gamma^*)](\hat{\theta} - \theta^*)$ to the previous inequality to get:

$$\lambda \|\hat{\theta} - \theta^*\|_2^2 \leq \mathbb{E}[(w(\hat{g}, \hat{\gamma}) - w(g^*, \gamma^*))(\hat{\theta} - \theta^*)] \quad (26)$$

We expand the target difference $w(\hat{g}, \hat{\gamma}) - w(g^*, \gamma^*)$:

$$\begin{aligned} w(\hat{g}, \hat{\gamma}) - w(g^*, \gamma^*) &= \hat{g} + \hat{\gamma}(\mathbf{z} - \hat{g}) - (g^* + \gamma^*(\mathbf{z} - g^*)) \\ &= (\hat{\gamma} - \gamma^*)(\mathbf{z} - g^*) + (\hat{g} - g^*)(1 - \gamma^*) + (\hat{g} - g^*)(\gamma^* - \hat{\gamma}) \end{aligned} \quad (27)$$

when put into Eq. (26), the first and second terms vanish because $\mathbb{E}[\mathbf{z} - g^* | \mathbf{y}] = 0$ and $\mathbb{E}[1 - \gamma^* | \mathbf{y}] = 0$ respectively. Therefore, we get (after taking the absolute value and noting that the LHS is non-negative):

$$\lambda \|\hat{\theta} - \theta^*\|_2^2 \leq |\mathbb{E}[(\hat{g} - g^*)(\hat{\gamma} - \gamma^*)(\hat{\theta} - \theta^*)]| \quad (28)$$

Using Holder's inequality with coefficients $(1/4, 1/4, 1/2)$:

$$\lambda \|\hat{\theta} - \theta^*\|_2^2 \leq \|\hat{g} - g^*\|_4 \|\hat{\gamma} - \gamma^*\|_4 \|\hat{\theta} - \theta^*\|_2 \quad (29)$$

However, since $\hat{\theta}$ minimizes the empirical loss, not the population loss, we need to add back the empirical process term:

$$\lambda \|\hat{\theta} - \theta^*\|_2^2 \leq \text{Rate} + \|\hat{g} - g^*\|_4 \|\hat{\gamma} - \gamma^*\|_4 \|\hat{\theta} - \theta^*\|_2 \quad (30)$$

Now we apply Cauchy-Schwarz inequality to the RHS's second term:

$$\begin{aligned} \lambda \|\hat{\theta} - \theta^*\|_2^2 &\leq \text{Rate} + (2/\lambda) \|\hat{g} - g^*\|_4^2 \|\hat{\gamma} - \gamma^*\|_4^2 \\ &\quad + (\lambda/4) \|\hat{\theta} - \theta^*\|_2^2 \\ &\leq \text{Rate} + (2/\lambda) \|\hat{g} - g^*\|_4^4 + (\lambda/4) \|\hat{\theta} - \theta^*\|_2^2 \\ \|\hat{\theta} - \theta^*\|_2^2 &\leq \text{Rate} + O(\|\hat{g} - g^*\|_4^4) \end{aligned} \quad (31)$$

we have used Assumption. 3. Finally, we can invoke Assumption. 4 to convert Rate to $O(1/n)$, achieving the desired claim.

Supplemental Experiment Results

Comparison with other robust baselines. We compare DeDPO with 3 other baselines: the label smoothing loss by the original DPO author [35], IPO [1] and a recent distributionally robust optimization (DRO) [59]. As discussed, these works either assume a structural noise model or use DRO to guard against worst-case scenario, which is different from our setting where we have a set of labeled data to guide the correction of the synthetically-labeled data (as in Proposition. 2). Therefore, to be fair to these baselines, we also construct synthetic labels from randomly corrupted ground truth, which is ideal for their setting. In particular, as Qwen synthetic labels for pickapic FiFA-5k have an accuracy of 80%, we randomly flip 20% of the ground truth labels. Tab. 5 shows that our DeDPO still beats other baselines and the non-robust DPO with synthetic pref. by a wide margin in both synthetic sources. Specifically, in the Qwen setting, our method is higher than the highest baseline Label Smoothing by 0.27 in PickScore, and even the non-robust DPO is better than all robust baselines, showing that they are not suitable for our setting. In the 20% flipped setting, the non-robust DPO with synthetic pref. and our DeDPO degrade significantly, yet while DPO is now lower than all baselines, DeDPO remains higher than all baselines, being 0.06 higher than the highest baseline DRO in PickScore.

Table 5. Comparison with other robustness methods for DPO using dataset FiFA-5k and model SD1.5. The metric is PickScore.

Synthetic Source	DRO [59]	Label Smoothing [35]	IPO[1]	DPO	DeDPO
Qwen	21.63	21.64	21.52	21.71	21.91
20% Flip	21.66	21.62	21.51	21.49	21.72

Synthetic Preference Bias. In the preceding paragraph, we have said that our setting of synthetic preference is different from noisy (flipped) labels, and our robustness method

is much more suitable for the synthetic preference setting, although it still performs well on the other setting. The reason is that the synthetic preference's discrepancy with the human preference is not random noise, but rather systematic bias. This means that there are identifiable patterns in the way the synthetic preference makes errors. Obviously, the noise-model approaches are not suitable for this kind of error. To correct for bias, we need information about the true distribution that we want. Thus, we see that using a small set of high quality labeled data is an obvious solution in retrospect. With the debiased loss, DeDPO is thus able to enhance robustness to synthetic preference. To verify that there are identifiable systematic bias in the synthetic preference, we perform a detailed bias analysis comparing label generation between the synthetic annotator (Qwen-VLM) and human preference. By examining the prompts that yield disagreement in labels, we confirmed that the discrepancies are not random. There exist systematic patterns in how the synthetic model judges an image differently than a human. This systematic bias can stem from various sources, including the prompt engineering techniques used during the synthetic label generation process. Fig. 5 demonstrates one such specific bias identified in our synthetic labels along with our detailed analysis.

Robustness against randomization. To verify the robustness of DeDPO's performance gains over DPO and eliminate the dependency on randomness, we performed 15 independent test runs with different random seeds. Across both SD1.5 and SDXL architecture, DeDPO exhibits variance comparable to or smaller than all DPO variants. For SD1.5, the standard deviation (σ) of PickScore across runs is $\sigma_{\text{DeDPO}} = 0.0076$. This is lower than all DPO variants, with the minimum is $\sigma_{\text{DPO+25\%}} = 0.0095$. Similarly, for SDXL, DeDPO demonstrates superior stability with a standard deviation of only $\sigma_{\text{DeDPO}} = 0.0094$, compared to the corresponding DPO's minimum baselines $\sigma_{\text{DPO+pseudo}} = 0.0112$. Moreover, DeDPO consistently maintains higher PickScores across all seeds and models. These results validate that DeDPO performance gains are robust against random initializations.

Benchmarking across different preference label sources. Our main results compared DeDPO and DPO when training on synthetic preferences from different annotators, comparing on PickScore. Tab. 6 complements this comparison by providing further benchmarking with the HPSv2 Average score [60] (referred to as HPSv2 for brevity, representing the average across its four categories) and Aesthetic score (AS). Across all three synthetic preference sources—self-training, CLIP, and Qwen-VLM—DeDPO consistently outperforms vanilla DPO on all scores. Significantly, we see a 2.58% HPSv2 improvement on CLIP, and a 1.87% on AS with Qwen-VLM pseudo label. This observation confirms

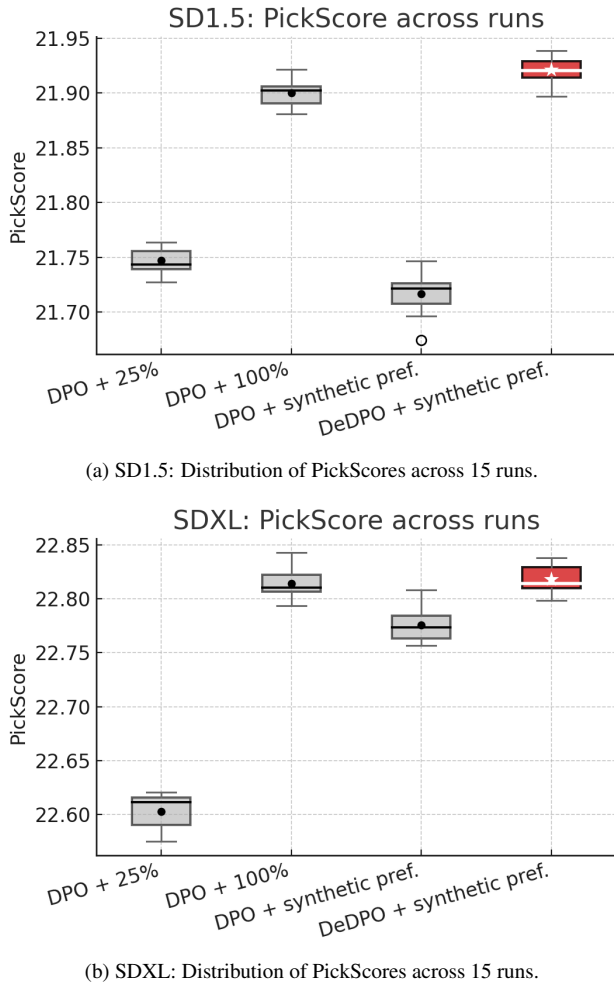


Figure 4. Comparison of PickScore distributions for different preference-learning strategies with SD1.5 (top) and SDXL (bottom).

our hypothesis that DeDPO enhances the efficacy of training processes that rely on synthetically generated preference labels.

Table 6. Benchmarking DeDPO and DDPO on different synthetic preference sources. Our 3 scores: PickScore (PS), HPSv2, and Aesthetic score (AS))

	DPO			DeDPO		
	PS (↑)	HPSv2 (↑)	AS (↑)	PS (↑)	HPSv2 (↑)	AS (↑)
Self-training	21.79	27.74	5.36	21.84	27.92	5.41
CLIP	21.46	27.06	5.27	21.90	27.77	5.40
Qwen-VLM	21.71	27.38	5.33	21.91	27.80	5.43

Scalability. We argue that DeDPO is suitable for training on synthetic label preferences at scale. In Tab. 7 we study how performance changes when we keep the number of high quality labeled preference pairs fixed at 1k2, while increasing the amount of synthetic preferences rated

on Qwen-VLM. Similar to the findings in the previous section, we provide further evidence of our method’s scalability using PickScore (PS), Aesthetic Score (AS), and HPSv2 metrics. The results show that DPO exhibits marginal, non-monotonic gains as the synthetic data increases. For instance, the PS for DPO fluctuates between 21.69 and 21.82, and HPSv2 ranges between 27.29 and 27.61, indicating that DPO remains largely stagnant when scaled with more synthetic labels, exhibiting noticeable degradation at the highest scale. In contrast, DeDPO consistently achieves superior performance compared to DPO across all synthetic scales. Crucially, while a slight trend of degradation is observed at the largest scale (similar to DPO), DeDPO’s overall performance remains highly stable across the 3.8k to 98.8k span. The total variation (maximum Δ) for DeDPO is minimal: PS varies only by 0.07 points and HPSv2 by just 0.10 points. This comparative analysis confirms that DeDPO possesses a significantly higher degree of robustness to the quantity of unlabeled preferences, effectively leveraging large synthetic pools without incurring substantial performance degradation.

Table 7. Comparison of DPO and DeDPO when using 1k2 high quality labeled preference pairs and increasing the number of synthetic preference pairs from Qwen-VLM.

Unlabel. size	DPO			DeDPO		
	PS (↑)	HPSv2 (↑)	AE (↑)	PS (↑)	HPSv2 (↑)	AE (↑)
3k8	21.71	27.39	5.33	21.91	27.80	5.43
8k8	21.82	27.61	5.41	21.92	27.76	5.42
38k8	21.70	27.37	5.33	21.96	27.76	5.42
98k8	21.69	27.29	5.32	21.89	27.70	5.41

Scaling training dataset size. Tab. 8 analyzes how performance changes as we increase the total number of preference pairs while keeping the labeled–unlabeled ratio fixed at 25%–75%. As in the main paper, DPO remains almost flat across dataset sizes, with PickScore (PS) and HPSv2 showing only minor fluctuations around a similar level. In contrast, DeDPO consistently outperforms DPO at every scale, with gains of roughly 0.1–0.2 in PS, 0.2–0.5 in HPSv2, and 0.05–0.1 in Aesthetic score (AE).

Table 8. Comparison of DPO and DeDPO across training set sizes, with the labeled–unlabeled preference ratio fixed at 25%–75%.

Size	DPO			DeDPO		
	PS (↑)	HPSv2 (↑)	AE (↑)	PS (↑)	HPSv2 (↑)	AE (↑)
5K	21.71	27.39	5.33	21.91	27.80	5.43
10K	21.76	27.53	5.35	21.86	27.73	5.40
50K	21.76	27.43	5.35	21.85	27.89	5.40
100K	21.70	27.32	5.33	21.87	27.66	5.40

Qualitative results. Fig. 6 and Fig. 7 provide more examples comparing DeDPO + synthetic preferences (ours) against three DPO variants (DPO + synthetic pref., DPO +

Prompt (text)	Model Preference	Human Preference
a portrait of an old coal miner in 19th century, beautiful painting with highly detailed face by greg rutkowski and magali villanueve		
a young sophisticated drinking black woman, gold and filigree, cozy dimly-lit 1920s speakeasy bar, drinking at the bar, dystopian retro 1920s soviet vibe, relaxed pose, pixie cut, wild, highly detailed, digital painting, artstation, sharp focus, illustration, detailed painterly digital art style by Joe Fenton, vibrant deep colors, 8k octane beautifully detailed render, post-processing, extremely hyper-detailed, Art Nouveau, masterpiece		
futuristic real realistic 4k full-frame mirrorless photo detailed city casablanca morocco cyberpunk street render concept art new historic blend market		
A painting of a wise elder from kenya by lynette yiadom-boakye . dramatic angle, ethereal lights, details, smooth, sharp focus, illustration, realistic, cinematic, artstation, award winning, rgb, unreal engine, octane render, cinematic light, macro, depth of field, blur, red light and clouds from the back, highly detailed epic cinematic concept art cg render made in maya, blender and photoshop, octane render, excellent composition, dynamic dramatic cinematic		

Figure 5. **Comparison of preference mechanisms between synthetic (Qwen-VLM) and human labels.** Qwen-VLM prioritizes semantic coherence and aesthetic adherence, strictly following artistic style constraints. However, it exhibits limited grounding in photorealism tokens, often failing to associate terms like "8k" or "hyper-detailed" with realistic texturing. Conversely, human preferences show a strong bias toward photorealistic fidelity; human evaluators frequently overlook hallucinations or ignored constraints (e.g., missing details, specific styles like "painting") if the resulting image appears realistic.

25% labeled, and DPO + 100% labeled). Qualitative examination demonstrates that DeDPO, when trained on synthetic preferences, consistently produces images that show stronger prompt following than all DPO variants. Specifically, DeDPO excels at detecting and accurately rendering small, fine-grained details in the prompt (e.g., the horns on

the Japanese girl, the wombat's raised hands, the wizard's hourglass iconography). Crucially, this improved adherence to detail is achieved while maintaining strong aesthetic coherence comparable to the performance of the theoretically upper-bound baseline, DPO trained on 100% high-quality labeled data.

A close-up photo of a wombat wearing a red backpack and raising both arms in the air. Mount Rushmore is in the background.



DeDPO + synthetic pref.

A black and orange yin-yang symbol with tiger's heads instead of circles.



DPO + synthetic pref.



DPO + 25%



DPO + 100%



A Japanese girl with small horns, long hair, and an elegant smile is praying on the floor of a destroyed church, portrayed in detailed artwork by Yoji Shinkawa.



A bowl of soup that looks like a monster knitted out of wool.



Figure 6. Qualitative comparison across different training schemes. Columns show four example prompts (top), and rows show generations from DeDPO + synthetic pref., DPO + synthetic pref., DPO + 25% labeled, and DPO + 100% labeled. DeDPO matches the aesthetic preference from the upper-bound model DPO + 100%, while improving prompt following on finer-grain detail of the images e.g., horns on the Japanese girl, or the raised hands of the Wombat. This improve the quality of the images generated sustainably, provide more depth to the photos.

Image of the Sandman, an ancient wizard with hour glass, casting beautiful dreams.

A woman with long hair next to a luminescent bird.

Cyberpunk girl sitting in a box in advanced anime digital art.

A photo of llama wearing sunglasses standing on the deck of a spaceship with the Earth in the background

DeDPO + synthetic pref.



DPO + synthetic pref.



DPO + 25%



DPO + 100%



Figure 7. Qualitative comparison across different training schemes. Columns show four example prompts (top), and rows show generations from DeDPO + synthetic pref. (ours), DPO + synthetic pref., DPO + 25% labeled, and DPO + 100% labeled. DeDPO produces images that better match fine-grained prompt details (e.g., subject attributes, composition, and style) while maintaining high aesthetic quality. For example, the Cyberpunk girl shows improvement in lighting consistency, the llama photo shows a subtle earth in the background.